ACS APPLIED MATERIALS & INTERFACES
Research Article
www.acsami.org

Effect of Blocking Layer to Boost Photoconversion Efficiency in ZnO Dye-Sensitized Solar Cells

Gurpreet Singh Selopal,[†,‡] Nafiseh Memarian,[§] Riccardo Milan,[†,‡] Isabella Concina,*[,†,‡] Giorgio Sberveglieri,[†,‡] and Alberto Vomiero*[,†,‡]

[†]SENSOR Lab, Department of Information Engineering, University of Brescia, Via Valotti 9, 25133 Brescia, Italy
[‡]CNR-INO SENSOR Lab, Via Branze 45, 25123 Brescia, Italy
[§]Faculty of Physics, Semnan University, Semnan, Iran

Ⓢ *Supporting Information*

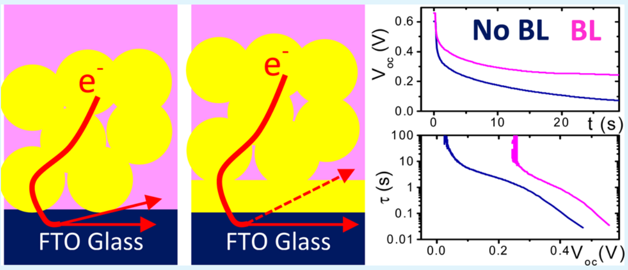

ABSTRACT: The effect of a ZnO compact blocking layer (BL) in dye-sensitized solar cells (DSSCs) based on ZnO photoanodes is investigated. BL is generated through spray deposition onto fluorine-doped tin oxide (FTO) conducting glass before the deposition of a ZnO active layer. The functional properties of dye-sensitized solar cells (DSSCs) are then investigated as a function of the thickness of the BL for two different kinds of ZnO active layer, i.e., hierarchically self-assembled nanoparticles and microcubes composed of closely packed ZnO sheets. Presence of BL leads to the improvement of photoconversion efficiency (PCE), by physically insulating the electrolyte and the FTO. This effect increases at increasing BL thickness up to around 800 nm, while thicker BL results in reduced cell performance. Remarkable increase in J_{sc} is recorded, which doubles as compared to cells without blocking layer, leading to PCE as high as 5.6% in the best cell under one sun irradiation (AM 1.5 G, 100 mW cm^{-2}). Electrochemical impedance spectroscopy (EIS) elucidates the mechanism boosting the functional features of the cells with BL, which relies with enhanced chemical capacitance together with an almost unchanged recombination resistance, which are reflected in an increased electron lifetime. The results foresee a straightforward way to significantly improve the performance of ZnO-based DSSCs.

KEYWORDS: *zinc oxide, dye sensitized solar cells, blocking layer, electron recombination*

■ INTRODUCTION

Dye-sensitized solar cells (DSSCs),[1−3] belonging to the wider class of excitonic solar cells, are attractive devices for large-area-scalable, low-cost, and environmentally compatible solar energy conversion, hence representing a concrete alternative to commercial solid-state semiconductor solar cells. However, their photoconversion efficiency still remains below 13% because of the intrinsic limitation in charge transport.[4] The photoanode of a DSSC consists of a mesoporous oxide semiconductor film with high specific surface area deposited on a transparent conducting oxide (TCO).[5−7] The highest photoconversion efficiency (PCE) has been achieved with film typically 10−15 μm thick consisting of 20 nm TiO_2 nanocrystallites in size, sensitized by different dye molecules (12.3% for zinc porphyrin dye[4] and 11.1% for the most common N719 dye[8]), in which large TiO_2 particles (200−400 nm in size) can act as scattering centers. Other *n*-type metal oxide semiconductors can be used in place of TiO_2; zinc oxide is the most promising[9−12] because of its electronic band structure (very similar to TiO_2) and higher electron mobility (see ref 13 and references therein). The preparation of the photoelectrode is crucial to enhance PCE[14] and various strategies have been suggested to tailor the geometry as well as the structure of the network, as for example the use of nanowires,[15−20] mixture of nanowires and nanoparticles,[21,22] hybrid structures,[23] or nanorod-nanosheet hierarchical assembly.[12,24] Recently, light confinement in hierarchically assembled networks has been demonstrated, in which large aggregates of nanocrystallites act as light scattering centers, while keeping high specific surface area.[11,25−27] We obtained quite larger PCE (7.5%) by introducing a blocking layer (BL) with the overall result of inhibiting electron recombination during the transport and collection process.[28]

BL was applied in TiO_2 DSSCs as barrier layer at fluorine-doped tin oxide glass (FTO)/TiO_2 interface to increase PCE.[29−32] The main effect of the BL on the functional properties of the cells was a significant increase of J_{sc}. Interpretation of the results was not conclusive: Park and coworkers demonstrated that increased performances were closely related to the charge transfer resistance at the blocking layer/electrolyte interface, and that electron loss near the FTO substrate was effectively prevented by the presence of the BL.[31]

Received: March 10, 2014
Accepted: June 18, 2014
Published: June 18, 2014

dx.doi.org/10.1021/am501360a | *ACS Appl. Mater. Interfaces* 2014, 6, 11236−11244

Fabregat and co-workers, instead, found that the main factor producing higher PCE was the improved physical contact between the coated FTO substrate and the TiO_2 film.[32]

However, thick TiO_2 BL generates a series resistance and an electron barrier that reduces the charge collection efficiency. Therefore, the advantage gained by using BL is lost if the BL layer is too thick, and, generally, the increase in PCE does not exceed the 25% in TiO_2 DSSCs with quite low PCE (4.83% PCE for the reference cell in ref 32) and the 6% in TiO2 DSSCs with higher PCE (7.35% PCE for the reference cell in ref 31).

For these reasons, use of BL in TiO_2 DSSCs has limited practical applications.

In the scheme, the main processes occurring in a DSSC according to the present scheme: (red line) enhanced light trapping as a result of the hierarchical agglomeration of ZnO and Levy flights of the light;[33] (blue line) electron path toward FTO and electron back reaction from the FTO to the electrolyte.

For ZnO DSSCs, instead, we demonstrate here that limitation in BL thickness is not an issue, and that BL as thick as several hundreds of nm can be successfully applied. Such thick layer allows to increase more than twice PCE, which significantly differ from typical increase obtained in other recent works on ZnO DSSCs.[34] In addition, we demonstrate that application of BL has general validity for ZnO DSSCs, independently of the kind and morphology of ZnO active layer.

Here we report a systematic investigation of the role of the BL in inhibiting electron back recombination in an operating DSSC based on ZnO photoanode (the main concept of the effect of the BL in an operating DSSC is illustrated in Scheme 1).

Scheme 1. Scheme of the proposed DSSC

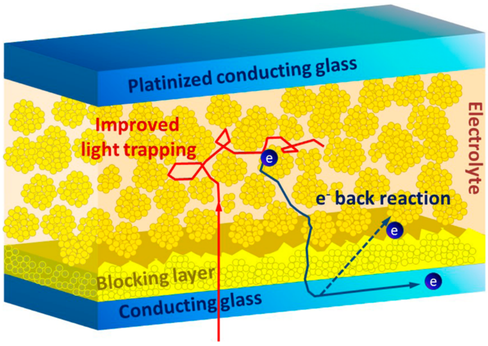

The complete photoanode is based on a layer-by-layer stacking of suitably engineered structures, each of which designed to improve specific functionalities of the cell. Light managing and electron transport and collection are in particular optimized, hence enhancing the overall photoconversion efficiency.

The ZnO BL is produced through spray deposition, a vacuum-free, fast and large area-scalable deposition technique, delivering a compact and transparent film, deposited atop the FTO glass, which acts as physical insulator element between the FTO and the electrolyte, thus enhancing, as we will see below, the overall electron lifetime, recognized among the critical parameters affecting charge collection and photoconversion efficiency.[29,35,36] The scheme (not to scale) illustrates the recombination losses in DSSCs, mainly occurring at the interface between the FTO and the electrolyte, which penetrates the large interpore volumes of the photoanode. The compact BL thus acts as a physical barrier, separating the FTO from the electrolyte We will show that, differently from traditional TiO_2 photoanodes, quite thick ZnO BLs can be applied resulting in increased PCE as a function of BL thickness. The presence of BL does not negatively affect the series resistance of the solar cell thanks to the quite high bulk electron conductivity of ZnO, whereas in TiO_2-DSSCs high resistivity of TiO_2 limits the full exploitation of the potential of the BL geometry.[32]

To provide solid demonstration of the role of the BL, we apply two different active layers, namely ZnO hierarchically self-organized nanoparticles[28] and ZnO microcubes composed of ZnO nanosheets. Both of these layers were specifically engineered to feature high light scattering,[33,37] strategic for inducing long residence time of the light inside the photoanode (thus enhancing the absorption probability by dye molecules) while keeping the high specific surface typical of mesoporous films (critical for dye uptake).

■ EXPERIMENTAL SECTION

Spray pyrolysis of ZnO blocking layer. Spray pyrolysis for the deposition of the BL was applied as follows:[28] zinc acetate dihydrate is used as ZnO precursor (0.24 M, 25 mL methanol/water, 2:1 v/v) and sprayed using N_2 carrier gas at pressure of 0.40 bar on an FTO glass (sheet resistance 10 Ω/□) kept at 250 °C. The amount of sprayed solution was 0.38 mL s^{-1}. Typical process is based on a series of spray cycles of fixed duration (10 s) followed by 5 s stops. The sprayed amount is around 3.8 mL per cycle, corresponding to a thickness of 200 nm/cycle. For the preparation of incomplete BL (resulting in partial coverage of the FTO), spray deposition parameters were changed as it follows: pressure 0.27 bar, spray rate 0.17 mL s^{-1}.

Oxidation of zinc acetate dihydrate on the hot FTO glass induced the formation of the blocking layer. Post deposition annealing was carried out in air at 450 °C for 30 min. Nozzle-to-sample distance was kept 37 cm.

Deposition of the active layers. *Hierarchical ZnO structures.* Hierarchical ZnO structures were directly generated on the TCO glass covered by the BL, as follows;[15] briefly, an ethanolic suspension of commercial ZnO nanoparticles (300 ± 90 nm in diameter, 0.5 g in 15 mL) and 40 mL of $Zn(CH_3COO)_2 \cdot 2\ H_2O$ 0.55 M (methanol/water, 3:1, V/V) were sprayed on a TCO glass at the same conditions described for ZnO BL. The amount of sprayed solution was 0.38 mL s^{-1}. Typical process is based on a series of spray cycles of fixed duration (10 s) followed by 5 s stops. The sprayed amount is around 3.8 mL per cycle.

Post-deposition annealing was carried out in air at 450 °C for 30 min.

ZnO Microcubes. ZnO microcubes were prepared by slowly dropping at room temperature 150 mL of an aqueous solution of NaOH (1 M) to a 0.04 M solution of $Zn(NO_3)_2$ x 6 H_2O in water under vigorous stirring. Once all the NaOH solution was mixed with the ZnO precursor solution, the reaction mixture was heated at 100 °C and kept boiling for 2 h, then let cool at room temperature. Obtained powder was filtered through filter paper and washed several times with deionized water, until neutrality (pH 7). Reaction product was dried in air at 95 °C for 6 h.

1.3 g of ZnO powder were then mixed with ethyl cellulose (0.5 g) and α-terpineol (1 mL) and dispersed in a mixture of ethanol/water (5/1, V/V). The mixture was then kept under vigorous stirring for 9 h in order to obtain a paste suitable for tape casting deposition on TCO glass.

All the oxide photoanodes were dye-sensitized by impregnation into a 5.0×10^{-4} M ethanolic solution of commercial Ru-based molecule dye N719 (Solaronix) for 2 h. After impregnation, samples were carefully washed with ethanol to remove unabsorbed dye.

Characterization of ZnO oxide layers. The BL and the active layer were characterized using standard techniques for determining their thickness (stylus profilometer), morphology (scanning electron microscope, SEM, carried out with a LEO1525 microscope) and transparency (UV−vis spectroscopy using a PG Instruments T80 spectrophotometer). Grazing incidence X-ray diffraction (GIXRD) using a Bruker D8 Advance diffractometer, CuKα X-rays source, λ = 1.542 Å, was applied to assess the crystalline structure of the BL after annealing.

Evaluation of Dye Loading. Dye loading on ZnO photoanode was measured by UV/vis spectrophotometry after calibration using diluted 0.1 M NaOH aqueous solutions of N719 dye. Adsorbed dye was completely removed from ZnO surface by washing with a 0.1 M NaOH aqueous solution.[38] Optical absorption spectra were collected at room temperature on a PG Instruments T80 spectrophotometer (1 cm quartz cuvettes were used for liquid samples).

Solar Cell Assembly and Characterization. DSSCs were fabricated by sandwiching the ZnO photoanode and the counter-electrode composed of Pt-sputtered FTO glass (Pt film thickness: 5 nm) using a 60 μm thick plastic spacer. The redox electrolyte contained 0.1 M LiI, 0.05 M I2, 0.6 M 1,2-dimethyl-3-n-propylimidazolium iodide, and 0.5 M 4-*tert*-butylpyridine in acetonitrile.

For each nominal condition of the solar cells (type of photoanode, layer thickness, presence of BL, BL thickness) we typically fabricated at least two DSSCs to evaluate the accuracy of the functional parameters and the reproducibility of the applied techniques. In the Supporting Information (Figures S2 and S3), we report the functional parameters of two DSSCs under the same nominal conditions for different thicknesses of the active layer. The typical uncertainty in the evaluation of the PCE is around 10% taking into account both the intrinsic errors of the measurement on a single cell and the reproducibility of the result on a nominally identical cell. Moreover, we report in the Supporting Information the uncertainty in the evaluation of PCE and the other functional parameters of the best operating devices with and without the BL.

The current−voltage (I−V) measurements were carried out without masking the solar cells using an ABET 2000 solar simulator under one sun simulated sunlight at AM 1.5G (100 mW cm^{-2}), calibrated with silicon reference cell. Active area of the cells was in the range 0.16−0.25 cm^2.

The electrochemical impedance spectroscopy (EIS) was carried out in dark conditions using a SOLARTRON 1260 A Impedance/Gain-Phase Analyzer, with an AC signal 20 mV in amplitude, in the frequency range between 100 mHz and 300 kHz. External bias in the range 0−900 mV was applied.

The transient open-circuit photovoltage decay (measured according to ref 39) was investigated to obtain information on electron lifetime.

RESULTS AND DISCUSSION

Blocking Layer and Photoanode Morphology. The first step for DSSC preparation is the generation of the BL through spray deposition. Then the deposition of the active layer follows. The two preparation steps of a typical photoanode are shown in Figure 1. The BL is composed of homogeneously distributed rough lamellae, a few tens of nanometers thick and with lateral dimensions in the submicrometer scale, oriented normal to the substrate plane.

The morphological characterization of the active layers is reported in images d and e in Figure 1, which illustrate the morphology of (i) the hierarchically assembled nanostructures and (ii) the microcubes, respectively. It is worth noting that the preparation procedure to obtain the BL and the hierarchically assembled structures is very similar: the only difference is the addition of commercial NPs to the solution of acetic acid before spraying: without commercial NPs in solution, we obtain the above-mentioned compact BL, while addition of NPs leads to the formation of the hierarchical nanostructures composed of microsized spheres, in which aggregation of nanosized NPs is clearly visible, as also documented in ref 28. The microcubes have rather different shape: they are constituted by assembled lamellae, hundreds of nanometers lateral size and about 20 nm thick (Figure 1e). The high specific surface of both the structures (hierarchical nanostructures and microcubes) is clearly visible, which is mandatory for high dye uptake and high optical density in the visible range after sensitization.

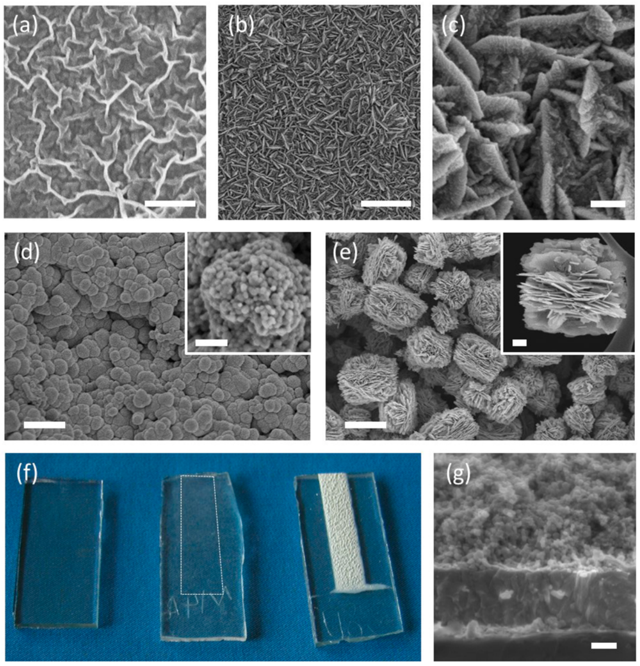

Figure 1. (a−c) Panoramic SEM images of the blocking layer at different magnifications. (a) Incomplete BL leaving part of uncovered FTO. (b) BL completely covering the FTO substrate. (c) Detail of the BL at higher resolution. The formation of 2D lamellae oriented normal to substrate surface (along the direction of film growth) is clearly visible. SEM images of the two different materials used as active layer: (d) hierarchically self-organized nanoparticles and (e) microcubes. In the insets of d and e: high-resolution SEM images highlighting the nanostructured arrangement of the active layers. (f) Sequence of (left to right) the glass substrate with FTO, FTO covered with the blocking layer (800 nm thick, region inside the white frame) and the completed photoanode. The high transparency of the FTO and of the blocking layer is clearly visible. (g) Cross-section of the complete DSSC including the FTO, the BL and the active layer composed of hierarchically self-assembled nanoparticles.[28] Scale bars: (a, b, d, e) 2 μm; (c, g, insets in d and e) 200 nm.

Optical Properties of the Photoanodes. The optical properties of the BL and the active layer are collected in (Figure 1f and Figure 2a, b). In the BL, the nanoshaped aggregations form a rather transparent layer in the visible range (Figure 1f and Figure 2) and cause limited light scattering in sufficiently thin films (absorbance below 0.4 at 500 nm for BL 740 nm thick). Absorbance of the BL at 370 nm and at 500 nm was investigated to gain information on absorbance close to the energy gap of the ZnO and on the competing light absorption of BL and N719 (which presents an absorption maximum at around 500 nm). Absorbance at 500 nm increases linearly with BL thickness (linear fit, black solid line in Figure 2b). Typically, smooth and compact ZnO films are transparent in the range of thickness of the present study.[40] Enhanced absorbance at 500 nm is here attributed to the scattering action of the BL at

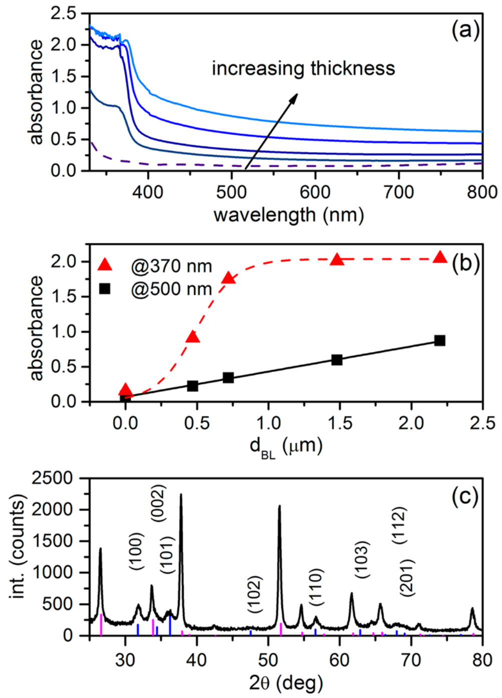

Figure 2. (a) UV−vis absorption spectra for various BL thicknesses (in the range 0.4−2.2 μm). The dashed spectrum refers to pure FTO glass. (b) Absorbance at 500 nm (black) and 370 nm (red) for the spectra collected in a. Absorbance at 500 nm increases linearly with the BL thickness, as expected, whereas it presents a sigmoidal growth in the UV region. (c) XRD pattern of ZnO BL on FTO. Blue, ZnO diffraction peaks according to JCPDS card 36−1451; pink, SnO_2 diffraction peaks according to JCPDS card 41−1445.

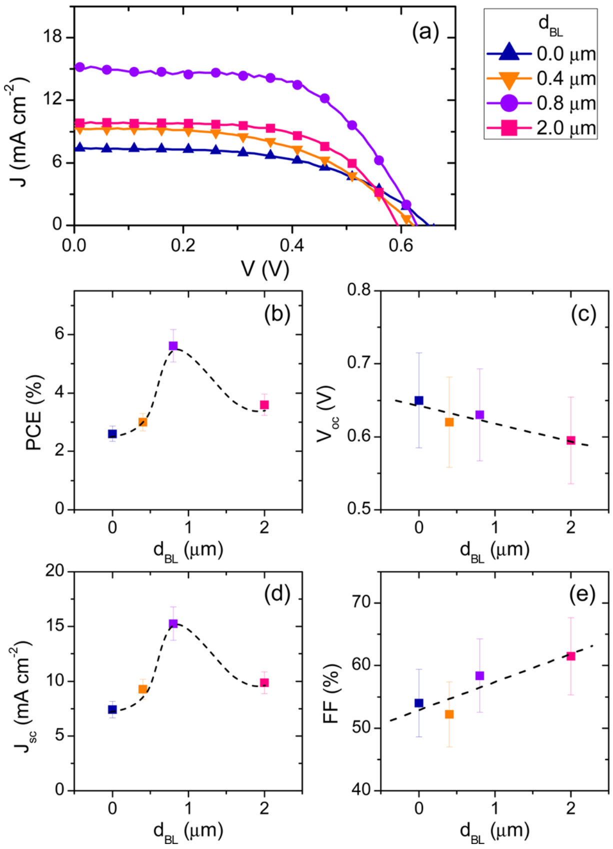

Figure 3. (a) Current density versus voltage curves of DSSCs composed of hierarchically structured nanoparticles for different thickness of the blocking layer (d_{BL}) under 1 sun illumination (AM 1.5G, 100 mW cm^{-2}). Functional features of the cells as a function of d_{BL}: (b) photoconversion efficiency (PCE); (c) open circuit photovoltage (V_{oc}); (d) short circuit photocurrent (J_{sc}); (e) fill factor (FF). Black lines in b−e are guides to the eye.

increased thickness, which is compatible with the submicrometer dimensions of the lamellae forming the BL. Further proof of this is the opacity of the BL, which appears pale white (not reported), at thickness above 2 μm. A steep increase in absorbance is recorded in the UV region at 370 nm, corresponding to energy gap absorption ($E_g \approx 3.3$ eV), perfectly fitted by a sigmoidal growth (sigmoidal fit, red dashed line in Figure 2b).

As far as the optical properties of the active layers, both the structures (hierarchically assembled nanoparticles and microcubes) form a strongly scattering film (see Figure 1f for the hierarchically assembled structures; the same holds for the microcubes): once deposited, the scattering action of the active layer makes the complete photoanode white.

Crystalline Structure of the BL. The XRD pattern of the ZnO BL deposited on FTO is reported in Figure 2(c). Reflections can be indexed according to the wurtzite crystal structure (Joint Committee on Powder Diffraction Standards—JCPDS card number 36−1451). Although visible, reflections from FTO do not interfere with identification of ZnO phase. The higher intensity of (100) peak with respect to (101), suggests possible preferential orientation of ZnO, in agreement with SEM observation, which testifies the presence of platelets vertically oriented with respect to substrate plane. The size of crystallites according to Scherrer equation resulted to be 11 nm.

Functional Characterization of the DSSCs. Evaluation of functional properties of cells shows the highly favorable effect of the blocking layer (Figure 3 reports the functional properties of a photoanode formed of hierarchically structured nanoparticles). The BL induces significant increase of J_{sc}, which reflects in enhanced PCE. According to consolidate literature in the field, such increase is typically caused by either enhanced optical density as a consequence of increased dye uptake,[41] or by inhibition of electron back reaction in the operating device.[31] We estimated the total amount of dye loaded in photoanodes with and without the BL, in order to assess the role of dye uptake and optical density in boosting photogenerated charges and collected photocurrent. The amount of loaded dye shows no significant differences between samples with and without BL, being dye loading equal to $(1.7 \pm 0.25) \times 10^{-7}$ mol mm^{-3} for samples without BL and $(1.9 \pm 0.30) \times 10^{-7}$ mol mm^{-3} for samples with BL. These results rule out the increase in optical density as potential cause of enhanced PCE, in agreement with recent results in the field.[34] Up to a thickness of about 800 nm, the thicker the BL, the most pronounced is its role in enhancing the obtained photocurrent, improving the photoconversion efficiency (PCE). PCE as high as 5.6% was obtained for the best operating device (photoanode thickness 15.5 μm and BL thickness 800 nm), which is promisingly high compared to similar results in literature.[42] Interestingly, the beneficial effect of the blocking layer amply compensates the drawback related to the presence of a compact film of increasing thickness, which could result, in principle, in increased electrical series resistance, as for the case of TiO_2 blocking layer.[32] As the resistance of a thin film scales with its thickness, one could expect a decreasing fill factor (FF) as a function of BL thickness, which is not the case in the present investigation (see Figure 3e): the potential drop due to the series resistance is indeed largely compensated by the increased charge collection.

Further proof of the effectiveness of the BL is inferred by the analysis of the solar cells as a function of the thickness of the active layer (Figure 4). The presence of the blocking layer guarantees almost doubling J_{SC} with respect to active layer deposited directly on the FTO, resulting in a significant enhancement of the photoconversion efficiency (the best cell with blocking layer has a PCE value of 5.6%, whereas 2.6% is obtained for the best cell without blocking layer). Such behavior was systematically confirmed in a wide range of photoanode thicknesses ranging between 10 and 50 μm, where PCE remains above 4%.

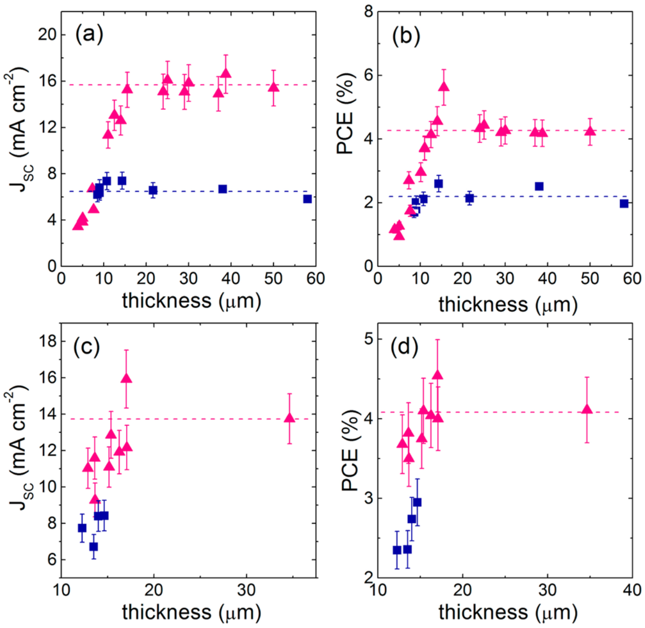

Figure 4. (a, c) J_{sc} and (b, d) PCE as a function of the thickness of the photoanode (blocking layer plus active layer) with (pink) and without (blue) optimized BL for hierarchically structured (a, b) nanoparticles and (c, d) microcubes.

In typical TiO_2 photoanodes, cell performances are optimized for photoanode thickness in the range 10−20 μm, and it was demonstrated that PCE versus thickness presents rather sharp peak around the maximum.[43] This behavior is due to the need of simultaneous optimization of optical and electrical properties of the photoanode, i.e., the optical density (which increases with film thickness) and collection of photogenerated charges, which decreases with thickness because of recombination processes.

For ZnO photoanodes, a broad range of thickness is reported to maximize PCE: Hosono et al. reported PCE as high as 2% in a 65 μm thick film, whereas thinner layers (50 and 60 μm) resulted in lower PCE because of the limited optical features (mainly light scattering).[44] Other authors reported maximum efficiencies for anode thickness around 15 μm (PCE = 7.5%),[28] 16 μm (PCE = 5.2% for D149 dye, PCE = 4.5% for N719),[45] 18 μm (PCE = 6.67%),[46] and 35.6 μm (PCE = 6.19% in a quasi-solid state configuration using ZnO microcubes).[41] In general, as in the present manuscript, optimum thickness for ZnO photoanodes is larger than for TiO_2. Such behavior in ZnO can be ascribed to higher electron mobility as compared to TiO_2, allowing the increase of layer thickness without electron loss due to recombination during charge transport. Anta and co-workers[47] experimentally measured an electron diffusion length larger than 80 μm in ZnO-based DSSCs sensitized with N719 dye, accounting for the increased optimum thickness in ZnO photoanodes. Our result is extremely important for the envisioned scale up of the process: in fact, on the basis of the functional characterization, up to 20% of variation of film thickness (which is an overestimate of what typical serigraphic methodology or tape casting processes guarantee) is compatible for effective exploitation of the devices. In addition, this result suggests that the main source of charge loss is independent from the thickness of the active layer (at least in the range 10−50 μm).

To consolidate these results, the best BL thickness (800 nm) was applied to the photoanode composed of microcubes, previously described and illustrated in Figure 1e.

Functional characterization of DSSCs exploiting microcubes as main layer provided similar results, as demonstrated in Figure 5: also in this case, application of ZnO BL highly enhances charge collection (an almost 40% J_{sc} increase is indeed measured) thus improving the overall PCE. The same behavior of PCE versus photoanode thickness is found also for ZnO microcubes, as reported in Figure 4c, d).

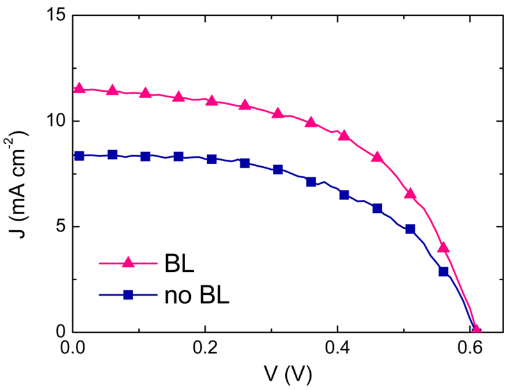

Figure 5. Current density versus voltage curves for DSSCs with and without BL using an active layer composed of microcubes of ZnO lamellae. Thickness of the active layer is 14 μm for both devices.

A quantitative comparison of the best solar cells with and without buffer layer is reported in Table 1.

Impedance Spectroscopy and Photovoltage Decay. We applied EIS to get rational understanding of charge dynamics in operating devices, and gave interpretation of the experimental results according to consolidated literature in the

Table 1. Functional Properties of the Best Solar Cells with and without the Buffer Layer Using Hierarchically Assembled Nanoparticles and Microcubes As Active Layers

active layer	BL	d^a (μm)	V_{oc} (V)	J_{sc} (mA cm^{-2})	FF (%)	PCE (%)
nanoparticles	no	14.5	0.650	7.40	54.0	2.6
	yes	15.9	0.63	15.25	58.4	5.6
microcubes	no	14.0	0.610	8.40	54.0	2.7
	yes	13.6	0.610	11.60	54.0	3.8

[a] Total thickness of the anode, including the BL. BL as thick as 800 nm is here considered.

field.[48,49] In Figure 6, we report the comparative analysis of two DSSCs with and without BL, whose photoanode is composed of microcubes. The EIS analysis was taken in dark condition applying an external bias in the range 0−900 mV, on a frequency range between 100 mHz and 300 kHz. The equivalent circuit to fit the experimental data (reported in Figure 6) is composed of RC pairs and a distributed element to fully characterize the oxide and its interfaces with electrolyte.[50] We consider an additional element (R_{BL} C_{BL} pair) in parallel to the distributed element in the case of cell with BL to take into account the presence of the BL. The impedance of the R_{CE} and C_{CE} pair is associated with the interface between the Pt counter electrode and the electrolyte (high frequency range $f > 1 \times 10^3$ Hz, referred to the semicircle at high frequency). The main semicircle (middle frequency range 1×10^3 to 1 Hz) is related to the charge transfer process at the sensitized oxide-electrolyte interface (R_{REC} and the $C\mu$).

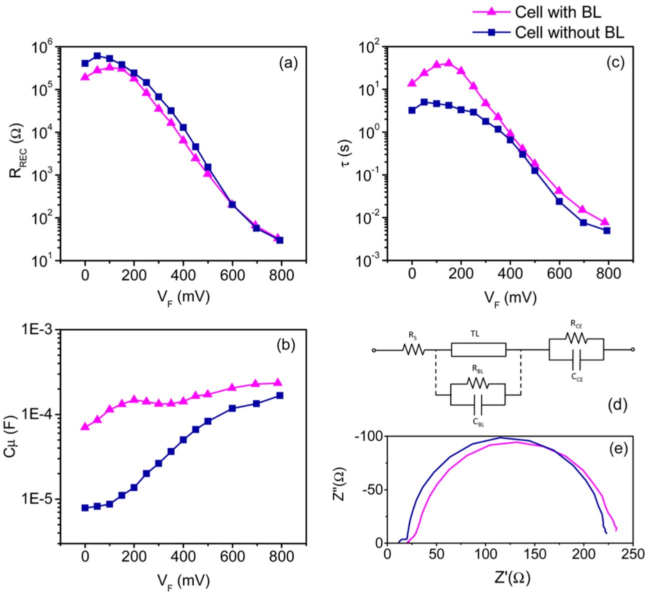

Figure 6. (a) Recombination resistance; (b) chemical capacitance and (c) electron lifetime as calculated by EIS analysis. (d) Equivalent circuit. (e) Nyquist plots of devices based on ZnO microcubes with and without the BL, under dark condition and around V_{oc}.

These parameters are critical in analyzing the charge recombination from oxide to electrolyte, which negatively affects PCE.

The full trends of recombination resistance and the chemical capacitance are reported in panels a and b in Figure 6, respectively, as a function of the potential drop at the sensitized electrode V_F in the range 0−900 mV. V_F is obtained after correcting the applied voltage for the drop at total series resistance evaluated from EIS data, according to consolidated literature.[32,51,52]

In the attempt to shine light on the actual role played by ZnO BL, a comparative analysis of R_{REC} and C_μ should be carried out. The recombination resistance is similar for the two cells,[32] with the exception of the region at low bias (0−200 mV), which however would not be significant since, as previously reported,[29] charge losses via FTO are negligible under short circuit conditions (due to close positions of Fermi levels FTO-electrolyte). What seems, on the contrary, worth noting here is that interposing of an additional oxide layer does not result in remarkable depression of R_{REC}. Analogous results for R_{REC} were found by Fabregat et al.[32] in TiO_2 DSSCs with thin BL.

The trend of chemical capacitance is markedly different whether the BL is present or not. C_μ pertaining to the device provided with BL is systematically higher than that of the cell without the BL, thus accounting for the corresponding higher photocurrent density.

According to the commonly accepted interpretation of the chemical capacitance,[53] three main regions can be identified. At high voltages (>800 mV) the chemical capacitance tends to surface Helmholtz capacitance of the MOX/electrolyte interface (very high potentials) and indeed curves corresponding to devices with and without BL are running toward convergence.

Huge differences are instead identified in the curves at medium and low potentials. Taken into account that the analyzed devices have similar thickness, the different capacitance identified for the devices does not correlated with an increase in the overall volume of the photoanodes. According to Bisquert's model, the region at low potential (up to about 200 mV) is dominated by the BL (and the CE, which is exactly the same in the two cases): a significant difference in slope is observed and in particular the curve pertaining to the device with BL increases the corresponding C_μ much faster than the cell not provided with BL. This steep slope would suggest a stronger tendency to charge accumulation.

Another relevant difference is observed at medium potentials (this region being dominated by the behavior of the oxide composing the anode): whereas the device without BL shows a typical DSSC behavior (continuous increase in C_μ with increasing potentials), the presence of BL dramatically changes the curve shape. A plateau is indeed observed in the potential range from 250 to 450 mV and a small capacitance peak, absent if the BL is absent, is present at around 200 mV: both these features are frequently associated with surface defects (which could be either dangling bonds or surface trap states).[54] The presence of surface trap states is typically detrimental from viewpoint of charge recombination: however, in this case, the increase in the absolute value of the capacitance and related lifetime amply compensates the effect of the surface states, whose presence is highlighted by the plateau, leading to increased performances in the cell with BL.

All the mentioned characteristics indicate a better skill of the device with BL in charge accumulation, ascribable to an increased density of states derived from the presence of BL, which account for the enhanced photocurrent density.

This point would probably deserve a more specific investigation, which is beyond the aim of the present study, but presented results strongly support the beneficial role exerted by the buffer layer.

The electron lifetime calculated using the equation $\tau = R_{REC} \times C_\mu$[47] further highlights the benefit of BL: electron lifetime in the cell with BL is indeed systematically higher (see Figure 6c).

Similar results were found by Park and co-workers[31] on TiO_2 DSSCs: the presence of the compact BL would protect from electron losses, which are found to increase at the increasing BL porosity, because of enhanced contact between the electrolyte and the FTO.

These results differ from the ones reported by Peter and co-workers on BL in TiO_2 DSSCs,[29] in which the ability of the BL to prevent the electron back reaction is excellent under short circuit conditions, but is limited under open circuit conditions.

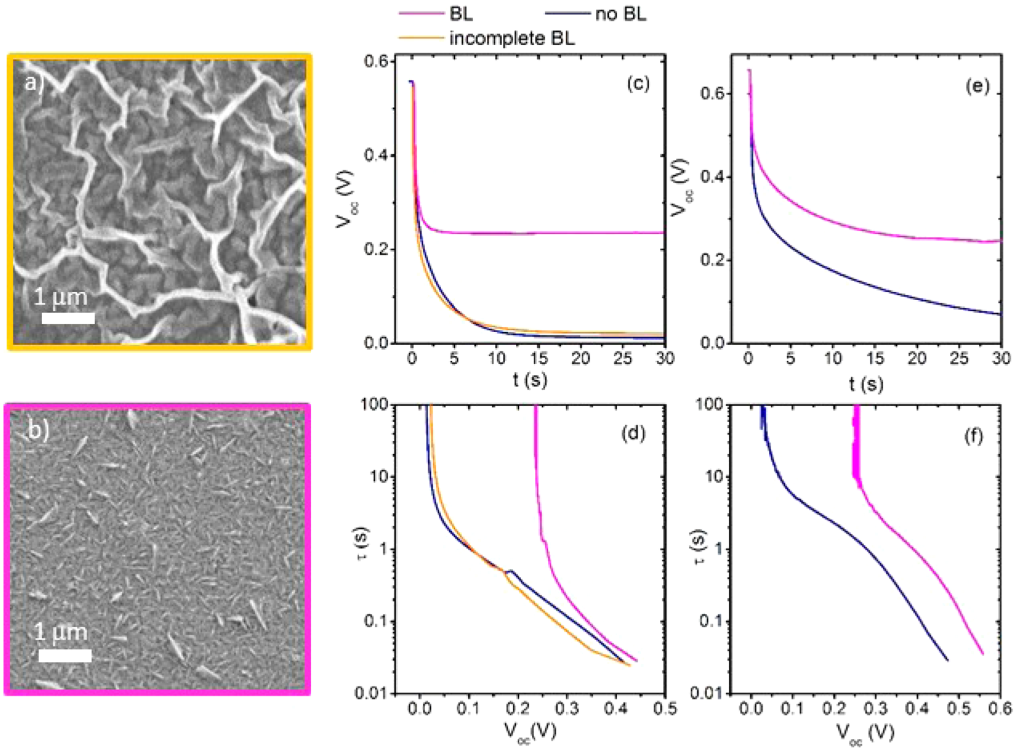

Figure 7. SEM images of (a) incomplete and (b) complete BL, (c, d) applied for transient photovoltage decay coupled with microcube active layers. Transient photovoltage decay and electron lifetime for DSSCs composed of (c, d) microcubes and (e, f) hierarchical nanoparticles. For microcubes, three different configurations were applied: (i) no BL, (ii) incomplete BL, (iii) complete BL. For hierarchical nanoparticles, solar cells with and without BL were considered.

Electron lifetime τ_e calculated from transient photovoltage decay according to eq 1[39] is reported in Figure 7 for DSSCs with and without BL composed of hierarchical nanoparticles, and for microcubes, in which three different BL configurations were applied: no BL, incomplete BL and complete BL. The main purpose of investigation of incomplete FTO coverage relies with the possibility of identifying the role of BL in insulating FTO from the electrolyte, inhibiting electron back reaction.

$$\tau_e = \frac{k_B T}{e}\left(\frac{dV_{oc}}{dt}\right)^{-1} \qquad (1)$$

As clearly seen, the direct contact between the electrolyte and the FTO drastically decreases τ_e, while complete coverage of FTO by the compact ZnO BL induces increased τ_e for both nanoparticles and microcubes. Rather interestingly, partial coverage of FTO seems having no effect in increasing electron lifetime, suggesting the important role of BL in conformal coverage of FTO. In fact, electron lifetime for partially covered and uncovered FTO is almost the same, as can be clearly seen in Figure 7c, d. In addition, the effect of increased lifetime is more pronounced for hierarchical nanoparticles, compared to microcube cells, which well-matches the results on PCE: in microcubes, in fact, increase in PCE is around 40%, while it is around 115% for hierarchical nanoparticles. Furthermore, it has to be pointed out that increased lifetime is maximized at low bias, whereas at high bias the effect tends to decrease. Similar behavior was found by Cameron and Peter,[29,30] who attributed the much lower value of τ_e to electron density decay in part via the FTO substrate. However, differently from what found in ref 29, transient photovoltage decay indicates increased lifetime for cells with BL even at high bias (above 400 mV). In the case of TiO_2, Peter and Cameron concluded that the BL was unable to block electron back reaction at high voltage and at open-circuit, resulting in poor increase of cell performances for device under operating conditions. In the present case, instead, the BL seems being able to inhibit back reaction, resulting in improved performances of the solar cell.

CONCLUSIONS

In conclusion, we carried out a systematic analysis on the role of the blocking layer in boosting photoconversion efficiency in ZnO-based dye sensitized solar cells. We demonstrated that application of ZnO blocking layer is effective irrespectively of the physical characteristics of the active layer (shape, size and size distribution). Effectiveness of the blocking layer increases up to an optimal thickness of 800 nm, delivering maximum photoconversion efficiency as high as 5.6% in the best cell, which is very high in the panorama of ZnO-based dye sensitized solar cells. The most significant effect of the presence of the blocking layer is to boost the short circuit photocurrent density from about 7.4 mA cm^{-2} to around 15 mA cm^{-2} in the best solar cell analyzed in this work. The increase in PCE is as high as 115% for hierarchical nanoparticle film and 40% in microcube photoanode, which is comparatively high with respect to PCE increase in TiO_2 DSSCs. EIS analysis seems indicating an improved charge accumulation ability, delivered by the ZnO BL, together with a good preservation of the overall R_{REC}, resulting in the noteworthy J_{sc} enhancement. In addition, we demonstrated that the blocking layer is effective in a broad range of photoanode thickness, which is technologically relevant for the scale up of solar cell. Transient photovoltage decay suggests increased electron lifetime for cells with BL, giving good explanation for increase in J_{sc}. The improvement seems to be related to a lower recombination, in the FTO/electrolyte interface, probably due to the stronger recombination in ZnO as compared with TiO_2. These results highly differ from the ones on TiO_2, in which the effect of a blocking layer is rather limited because of the detrimental high series resistance introduced in the cell; they give a rational way to improve the functional properties of ZnO photoanodes, and are critical for the development of a cheap, highly reproducible, and vacuum-free platform for the production of ZnO-based dye-sensitized solar cells.

■ ASSOCIATED CONTENT

Ⓢ Supporting Information

The effect of the BL on dye loading and the repeatability of the functional properties of the solar cells are reported . This material is available free of charge via the Internet at http://pubs.acs.org/.

■ AUTHOR INFORMATION

Corresponding Authors

*E-mail: isabella.concina@unibs.it.
*E-mail: alberto.vomiero@unibs.it.

Author Contributions

The manuscript was written through contributions of all authors. All authors have given approval to the final version of the manuscript.

Funding

F-Light Marie Curie EC contract 299490, WIROX EC contract 295216, Regione Lombardia (National Research Council Project “Tecnologie e Materiali per l’utilizzo efficiente dell’energia solare”).

Notes

The authors declare no competing financial interest.

■ ACKNOWLEDGMENTS

The authors thank Lei Jin and Federico Rosei for XRD data collection at INRS-EMT and Marta Maria Natile for useful discussions. Marco Musiani is acknowledged for fruitful discussion on EIS data analysis. A.V. acknowledges the European Commission for partial funding under the Contract F-Light Marie Curie 299490. The authors acknowledge the European Commission for partial funding under the contract WIROX 295216. I.C. acknowledges Regione Lombardia and National Research Council Project (“Tecnologie e Materiali per l’utilizzo efficiente dell’energia solare”) for partial funding. G.S.S. and R.M. acknowledge OIKOS s.r.l. for funding.

■ REFERENCES

(1) Gregg, B. A. Excitonic Solar Cells. *J. Phys. Chem. B* **2003**, *107*, 4688−4698.

(2) Gratzel, M. Photoelectrochemical Cells. *Nature* **2001**, *414*, 338−344.

(3) O’Regan, B.; Grätzel, M. A Low-Cost, High-Efficiency Solar Cell Based on Dye-Sensitized Colloidal Tio2 Films. *Nature* **1991**, *353*, 737−740.

(4) Yella, A.; Lee, H. W.; Tsao, H. N.; Yi, C. Y.; Chandiran, A. K.; Nazeeruddin, M. K.; Diau, E. W. G.; Yeh, C. Y.; Zakeeruddin, S. M.; Gratzel, M. Porphyrin-Sensitized Solar Cells with Cobalt (Ii/Iii)-Based Redox Electrolyte Exceed 12% Efficiency. *Science* **2011**, *334*, 629−634.

(5) Guo, P.; Aegerter, M. A. Ru(Ii) Sensitized Nb2o5 Solar Cell Made by the Sol-Gel Process. *Thin Solid Films* **1999**, *351*, 290−294.

(6) Keis, K.; Magnusson, E.; Lindstrom, H.; Lindquist, S. E.; Hagfeldt, A. A 5% Efficient Photo Electrochemical Solar Cell Based on Nanostructured Zno Electrodes. *Sol. Energy Mater. Sol. C* **2002**, *73*, 51−58.

(7) Stergiopoulos, T.; Arabatzis, I. M.; Cachet, H.; Falaras, P. Photoelectrochemistry at Sno2 Particulate Fractal Electrodes Sensitized by a Ruthenium Complex - Solid-State Solar Cell Assembling by Incorporating a Composite Polymer Electrolyte. *J. Photoch. Photobio. A* **2003**, *155*, 163−170.

(8) Nazeeruddin, M. K.; De Angelis, F.; Fantacci, S.; Selloni, A.; Viscardi, G.; Liska, P.; Ito, S.; Bessho, T.; Gratzel, M. Combined Experimental and Dft-Tddft Computational Study of Photoelectrochemical Cell Ruthenium Sensitizers. *J. Am. Chem. Soc.* **2005**, *127*, 16835−16847.

(9) Rao, A. R.; Dutta, V. Achievement of 4.7% Conversion Efficiency in Zno Dye-Sensitized Solar Cells Fabricated by Spray Deposition Using Hydrothermally Synthesized Nanoparticles. *Nanotechnol.* **2008**, *19*, 445712.

(10) Nagaya, S.; Nishikiori, H. Preparation of Dye-Adsorbing Zno Thin Films by Electroless Deposition and Their Photoelectrochemical Properties. *ACS Appl. Mater. Interfaces* **2013**, *5*, 8841−8844.

(11) Gao, R.; Liang, Z.; Tian, J.; Zhang, Q.; Wang, L.; Cao, G. Zno Nanocrystallite Aggregates Synthesized through Interface Precipitation for Dye-Sensitized Solar Cells. *Nano Energy* **2013**, *2*, 40−48.

(12) Gao, R.; Tian, J.; Liang, Z.; Zhang, Q.; Wang, L.; Cao, G. Nanorod-Nanosheet Hierarchically Structured Zno Crystals on Zinc Foil as Flexible Photoanodes for Dye-Sensitized Solar Cells. *Nanoscale* **2013**, *5*, 1894−1901.

(13) Zhang, Q.; Dandeneau, C. S.; Zhou, X.; Cao, G. Zno Nanostructures for Dye-Sensitized Solar Cells. *Adv. Mater.* **2009**, *21*, 4087−4108.

(14) Saito, M.; Fujihara, S. Large Photocurrent Generation in Dye-Sensitized Zno Solar Cells. *Energy Environ. Sci.* **2008**, *1*, 280−283.

(15) Law, M.; Greene, L. E.; Johnson, J. C.; Saykally, R.; Yang, P. D. Nanowire Dye-Sensitized Solar Cells. *Nat. Mater.* **2005**, *4*, 455−459.

(16) Baxter, J. B.; Aydil, E. S. Nanowire-Based Dye-Sensitized Solar Cells. *Appl. Phys. Lett.* **2005**, *86*, 053114.

(17) Varghese, O. K.; Paulose, M.; Grimes, C. A. Long Vertically Aligned Titania Nanotubes on Transparent Conducting Oxide for Highly Efficient Solar Cells. *Nat. Nanotechnol.* **2009**, *4*, 592−597.

(18) Vomiero, A.; Galstyan, V.; Braga, A.; Concina, I.; Brisotto, M.; Bontempi, E.; Sberveglieri, G. Flexible Dye Sensitized Solar Cells Using Tio2 Nanotubes. *Energy Environ. Sci.* **2011**, *4*, 3408−3413.

(19) Galstyan, V.; Vomiero, A.; Comini, E.; Faglia, G.; Sberveglieri, G. Tio2 Nanotubular and Nanoporous Arrays by Electrochemical Anodization on Different Substrates. *RSC Adv.* **2011**, *1*, 1038−1044.

(20) Galstyan, V.; Vomiero, A.; Concina, I.; Braga, A.; Brisotto, M.; Bontempi, E.; Faglia, G.; Sberveglieri, G. Vertically Aligned Tio2 Nanotubes on Plastic Substrates for Flexible Solar Cells. *Small* **2011**, *7*, 2437−2442.

(21) Vomiero, A.; Concina, I.; Natile, M.; Comini, E.; Faglia, G.; Ferroni, M.; Kholmanov, I.; Sberveglieri, G. Zno/Tio2 Nanonetwork as Efficient Photoanode in Excitonic Solar Cells. *Appl. Phys. Lett.* **2009**, *95*, 193104−193104−3.

(22) Yodyingyong, S.; Zhang, Q. F.; Park, K.; Dandeneau, C. S.; Zhou, X. Y.; Triampo, D.; Cao, G. Z. Zno Nanoparticles and Nanowire Array Hybrid Photoanodes for Dye-Sensitized Solar Cells. *Appl. Phys. Lett.* **2010**, *96*, 073115.

(23) Ko, S. H.; Lee, D.; Kang, H. W.; Nam, K. H.; Yeo, J. Y.; Hong, S. J.; Grigoropoulos, C. P.; Sung, H. J. Nanoforest of Hydrothermally Grown Hierarchical Zno Nanowires for a High Efficiency Dye-Sensitized Solar Cell. *Nano Lett.* **2011**, *11*, 666−671.

(24) Vomiero, A.; Concina, I.; Comini, E.; Soldano, C.; Ferroni, M.; Faglia, G.; Sberveglieri, G. One-Dimensional Nanostructured Oxides for Thermoelectric Applications and Excitonic Solar Cells. *Nano Energy* **2012**, *1*, 372−390.

(25) Cheng, H. M.; Hsieh, W. F. High-Efficiency Metal-Free Organic-Dye-Sensitized Solar Cells with Hierarchical Zno Photoelectrode. *Energy Environ. Sci.* **2010**, *3*, 442−447.

(26) Zhang, Q. F.; Cao, G. Z. Hierarchically Structured Photoelectrodes for Dye-Sensitized Solar Cells. *J. Mater. Chem.* **2011**, *21*, 6769−6774.

(27) Zhang, Q. F.; Chou, T. R.; Russo, B.; Jenekhe, S. A.; Cao, G. Z. Aggregation of Zno Nanocrystallites for High Conversion Efficiency in Dye-Sensitized Solar Cells. *Angew. Chem., Int. Ed.* **2008**, *47*, 2402−2406.

(28) Memarian, N.; Concina, I.; Braga, A.; Rozati, S. M.; Vomiero, A.; Sberveglieri, G. Hierarchically Assembled Zno Nanocrystallites for High-Efficiency Dye-Sensitized Solar Cells. *Angew. Chem., Int. Ed.* **2011**, *50*, 12321−12325.

(29) Cameron, P. J.; Peter, L. M. Characterization of Titanium Dioxide Blocking Layers in Dye-Sensitized Nanocrystalline Solar Cells. *J. Phys. Chem. B* **2003**, *107*, 14394−14400.

(30) Cameron, P. J.; Peter, L. M. How Does Back-Reaction at the Conducting Glass Substrate Influence the Dynamic Photovoltage Response of Nanocrystalline Dye-Sensitized Solar Cells? *J. Phys. Chem. B* **2005**, *109*, 7392−7398.

(31) Yoo, B.; Kim, K.-J.; Bang, S.-Y.; Ko, M. J.; Kim, K.; Park, N.-G. Chemically Deposited Blocking Layers on Fto Substrates: Effect of Precursor Concentration on Photovoltaic Performance of Dye-Sensitized Solar Cells. *J. Electroanal. Chem.* **2010**, *638*, 161−166.

(32) Goes, M. S.; Joanni, E.; Muniz, E. C.; Savu, R.; Habeck, T. R.; Bueno, P. R.; Fabregat-Santiago, F. Impedance Spectroscopy Analysis of the Effect of Tio2 Blocking Layers on the Efficiency of Dye Sensitized Solar Cells. *J. Phys. Chem. C* **2012**, *116*, 12415−12421.

(33) Barthelemy, P.; Bertolotti, J.; Wiersma, D. S. A Levy Flight for Light. *Nature* **2008**, *453*, 495−498.

(34) Guan, J.; Zhang, J.; Yu, T.; Xue, G.; Yu, X.; Tang, Z.; Wei, Y.; Yang, J.; Li, Z.; Zou, Z. Interfacial Modification of Photoelectrode in Zno-Based Dye-Sensitized Solar Cells and Its Efficiency Improvement Mechanism. *RSC Adv.* **2012**, *2*, 7708−7713.

(35) Kavan, L.; Gratzel, M. Highly Efficient Semiconducting Tio2 Photoelectrodes Prepared by Aerosol Pyrolysis. *Electrochim. Acta* **1995**, *40*, 643−652.

(36) Kruger, J.; Plass, R.; Gratzel, M.; Cameron, P. J.; Peter, L. M. Charge Transport and Back Reaction in Solid-State Dye-Sensitized Solar Cells: A Study Using Intensity-Modulated Photovoltage and Photocurrent Spectroscopy. *J. Phys. Chem. B* **2003**, *107*, 7536−7539.

(37) Wolf, P. E.; Maret, G. Weak Localization and Coherent Backscattering of Photons in Disordered Media. *Phys. Rev. Lett.* **1985**, *55*, 2696−2699.

(38) Thavasi, V.; Renugopalakrishnan, V.; Jose, R.; Ramakrishna, S. Controlled Electron Injection and Transport at Materials Interfaces in Dye Sensitized Solar Cells. *Mater. Sci. Eng., R* **2009**, *63*, 81−99.

(39) Zaban, A.; Greenshtein, M.; Bisquert, J. Determination of the Electron Lifetime in Nanocrystalline Dye Solar Cells by Open-Circuit Voltage Decay Measurements. *ChemPhysChem* **2003**, *4*, 859−864.

(40) Clagar, M.; Clagar, Y.; Ilican, S. The Determination of the Thickness and Optical Constants of the Zno Crystalline Thin Film by Using Envelope Method. *J. Optoelectron. Adv. Mater.* **2006**, *8*, 1410−1413.

(41) Shi, Y.; Zhu, C.; Wang, L.; Li, W.; Cheng, C.; Ho, K. M.; Fung, K. K.; Wang, N. Optimizing Nanosheet-Based Zno Hierarchical Structure through Ultrasonic-Assisted Precipitation for Remarkable Photovoltaic Enhancement in Quasi-Solid Dye-Sensitized Solar Cells. *J. Mater. Chem.* **2012**, *22*, 13097−13103.

(42) Anta, J. A.; Guillen, E.; Tena-Zaera, R. Zno-Based Dye-Sensitized Solar Cells. *J. Phys. Chem. C* **2012**, *116*, 11413−11425.

(43) Tan, B.; Wu, Y. Y. Dye-Sensitized Solar Cells Based on Anatase Tio2 Nanoparticle/Nanowire Composites. *J. Phys. Chem. B* **2006**, *110*, 15932−15938.

(44) Hosono, E.; Fujihara, S.; Kimura, T. Synthesis, Structure and Photoelectrochemical Performance of Micro/Nano-Textured Zno/Eosin Y Electrodes. *Electrochim. Acta* **2004**, *49*, 2287−2293.

(45) Ren, Y.; Zheng, Y.-Z.; Zhao, J.; Chen, J.-F.; Zhou, W.; Tao, X. A Comparative Study on Indoline Dye- and Ruthenium Complex-Sensitized Hierarchically Structured Zno Solar Cells. *Electrochem. Commun.* **2012**, *16*, 57−60.

(46) Sacco, A.; Lamberti, A.; Gazia, R.; Bianco, S.; Manfredi, D.; Shahzad, N.; Cappelluti, F.; Ma, S.; Tresso, E. High Efficiency Dye-Sensitized Solar Cells Exploiting Sponge-Like Zno Nanostructures. *Phys. Chem. Chem. Phys.* **2012**, *14*, 16203−16208.

(47) Guillen, E.; Peter, L. M.; Anta, J. A. Electron Transport and Recombination in Zno-Based Dye-Sensitized Solar Cells. *J. Phys. Chem. C* **2011**, *115*, 22622−22632.

(48) Bisquert, J.; Fabregat-Santiago, F.; Mora-Sero, I.; Garcia-Belmonte, G.; Gimenez, S. Electron Lifetime in Dye-Sensitized Solar Cells: Theory and Interpretation of Measurements. *J. Phys. Chem. C* **2009**, *113*, 17278−17290.

(49) Bisquert, J.; Cahen, D.; Hodes, G.; Ruhle, S.; Zaban, A. Physical Chemical Principles of Photovoltaic Conversion with Nanoparticulate, Mesoporous Dye-Sensitized Solar Cells. *J. Phys. Chem. B* **2004**, *108*, 8106−8118.

(50) Fabregat-Santiago, F.; Garcia-Belmonte, G.; Mora-Sero, I.; Bisquert, J. Characterization of Nanostructured Hybrid and Organic Solar Cells by Impedance Spectroscopy. *Phys. Chem. Chem. Phys.* **2011**, *13*, 9083−9118.

(51) Braga, A.; Giménez, S.; Concina, I.; Vomiero, A.; Mora-Seró, I. n. Panchromatic Sensitized Solar Cells Based on Metal Sulfide Quantum Dots Grown Directly on Nanostructured Tio2 Electrodes. *J. Phys. Chem. Lett.* **2011**, *2*, 454−460.

(52) Wang, Q.; Moser, J. E.; Gratzel, M. Electrochemical Impedance Spectroscopic Analysis of Dye-Sensitized Solar Cells. *J. Phys. Chem. B* **2005**, *109*, 14945−14953.

(53) Bisquert, J.; Fabregat-Santiago, F. Impedance Spectroscopy: A General Introduction and Application to Dye-Sensitized Solar Cells. In *Dye-Sensitized Solar Cells*; Kalyanasundaram, K., Ed. EPFL Press: Lausanne, Switzerland, 2010; Chapter 12.

(54) Huang, Q.; Li, F.; Gong, Y.; Luo, J.; Yang, S.; Luo, Y.; Li, D.; Bai, X.; Meng, Q. Recombination in Sno2-Based Quantum Dots Sensitized Solar Cells: The Role of Surface States. *J. Phys. Chem. C* **2013**, *117*, 10965−10973.